Cancer Nanotechnology

RESEARCH Open Access

Targeting and sensitizing MDR cancer by an MMP2 and pH dual-responsive ZnO-based nanomedicine

Qing Zhou[1,2†], Li Zhang[3†], Yujiao Li[2†], Jiao Wang[1], Xiaolu He[2], Jieyu Zhang[2], Youbei Qiao[4], Hong Wu[4*] and Lin Zhu[1*]

†Qing Zhou, Li Zhang and Yujiao Li contributed equally to this work

*Correspondence: wuhong@fmmu.edu.cn; lzhu@tamu.edu

[1] Department of Pharmaceutical Sciences, Irma Lerma Rangel School of Pharmacy, Texas A&M University, College Station, TX 77843, USA
[2] Department of Clinical Pharmacy, Jinling Hospital, Medical School of Nanjing University, Nanjing 210002, China
[3] Department of Prosthodontics, Nanjing Stomatological Hospital, Medical School of Nanjing University, Nanjing 210002, China
[4] Department of Medicinal Chemistry and Pharmaceutical Analysis, School of Pharmacy, Air Force Medical University, Xi'an 710032, China

Abstract

Zinc oxide nanoparticles (ZnO NPs) have been known as a therapeutic agent and drug delivery system for treating various diseases, including infectious diseases and cancer. However, due to the low biocompatibility, short in vivo half-life, and potential toxicity, the previous studies on ZnO NPs were mainly focused on their in vitro applications. The effective and safe ZnO NP-based systems which can be used for in vivo drug delivery have been rarely reported. In this study, we developed a novel dual-responsive hybrid ZnO NP (ZnO/DPPG/PEG-pp-PE) consisting of the ZnO NPs, phospholipid (DPPG), and enzyme-sensitive amphiphilic polymer (PEG-pp-PE), which could respond to both tumoral matrix metalloproteinase 2 (MMP2) and intracellular acidic pH, for tumor-targeted drug delivery and multidrug resistant (MDR) cancer treatment. The dual-responsive ZnO/DPPG/PEG-pp-PE could easily load the model drug, doxorubicin (DOX), and showed excellent physicochemical properties, stability, and MMP2 and pH dual sensitivity. The ZnO/DPPG/PEG-pp-PE/DOX showed the MMP2-dependent cellular uptake, enhanced cell penetration, and improved anticancer activity in the MDR cancer cells and their spheroids. In the MDR tumor-bearing mice, the ZnO/DPPG/PEG-pp-PE/DOX improved the biocompatibility, tumor targetability, and anticancer activity of DOX and ZnO without significant toxicity compared to the free DOX, ZnO/DOX, and nonsensitive ZnO NPs. The data suggested that the dual-sensitive ZnO-based nanomedicine could be a promising delivery system for targeted drug delivery and therapy against the MDR cancer.

Keywords: ZnO nanoparticles, MMP2-sensitive, pH-sensitive, Multidrug resistance, Doxorubicin

Introduction

Chemotherapy is one of the mostly used strategies for cancer treatment. However, tumor cells may develop a significant multidrug resistance (MDR) against chemotherapy drugs or other toxic agents after multiple dosing, which becomes one of the major reasons of treatment failure (Bukowski et al. 2020; Montazami et al. 2015). It is reported that over 90% of deaths in cancer patients are directly or indirectly attributed to the drug

resistance (Pluchino et al. 2012), making it a great challenge of cancer therapy. Therefore, it is of great interest to figure out an effective way to overcome the MDR and restore the tumor cell's susceptibility to chemotherapy drugs. The mechanisms of the MDR are complex and may include the oncogene mutations, impairment of drug metabolism, and overexpression of the transport proteins, which can be categorized into two major types, namely the efflux pump-mediated resistance and non-pump resistance (Szakács et al. 2006; Kunjachan et al. 2013). The ATP binding cassette (ABC) family of transmembrane transporter proteins is mainly responsible for the efflux pump-mediated drug resistance. They utilize the energy generated by the ATP hydrolysis to pump a variety of intracellular drugs out of the cell, resulting in the decreased intracellular drug concentration (Robey et al. 2018; Modok et al. 2006). The non-pump resistance is mainly attributed to the activation/overexpression of the anti-apoptotic proteins, such as Bcl-xL, Bcl-2, Survivin, NF-κB, etc. (Chauhan et al. 2012; An et al. 2017). Moreover, the conventional chemotherapy drugs lack the tumor specificity and usually kill both the cancerous and healthy cells in a nonselective manner (Iwamoto 2013; Boogaard et al. 2022). For example, doxorubicin (DOX), as a first-line chemotherapeutic drug, may cause severe side effects, including cardiotoxicity, bone marrow suppression, and testicular toxicity (Pugazhendhi et al. 2018).

Nanoparticle-based drug delivery system (NDDS) has emerged as an innovative and promising strategy for tumor-targeted drug delivery and circumvention of the MDR. Once loaded to the NDDS, anticancer drugs' cellular uptake may be enhanced via the efficient endocytosis and/or other internalization pathways, while its efflux may be inhibited due to the NPs' intracellular accumulation and sustained drug release (Liu et al. 2021; Patel et al. 2013; Su et al. 2021). Besides, NDDS can be designed to achieve the passive or active tumor targeting by utilizing the enhanced permeation and retention (EPR) effect of the tumor tissues and/or the binding affinity specific to the upregulated receptors on cancer cells, thus decreasing drugs' off-target toxicity and improving anticancer activity.

During the last two decades, a wide variety of nanomaterials have been explored to construct the NDDS for chemotherapy, including lipids, polymers, proteins, nucleic acids, and inorganic nanomaterials (Chaturvedi et al. 2019; Adir et al. 2020; Misra et al. 2010). Metal and metal oxide nanoparticles (NPs), such as gold NPs, iron oxide NPs, manganese oxide NPs, etc., are usually multifunctional and used in various biological applications. Among them, zinc oxide nanoparticles (ZnO NPs) have been promising in drug delivery, imaging/diagnosis, and treatment of infectious diseases and cancer, due to their unique physical and chemical properties (Anjum et al. 2021; Bisht and Rayamajhi 2016; Wiesmann et al. 2020). In a previous study, we demonstrated that ZnO NPs could work as a multifunctional and multitarget nanocarrier and nanomedicine and might have profound anticancer effects in cancer treatment (Wang et al. 2017). In particular, ZnO NPs can be readily dissolved and release Zn^{2+} at acidic pHs, which can be used as a pH-sensitive nanocarrier for intracellular drug release (David et al. 2012; Somu and Paul 2019). The accumulated intracellular Zn^{2+} can cause the mitochondrial dysfunction, ROS outburst and oxidative stress, lipid peroxidation and DNA damage, leading to the cell death (Guo et al. 2008). ZnO NPs can also upregulate the expression of the pro-apoptotic protein Bax and downregulate the expression of the anti-apoptotic protein

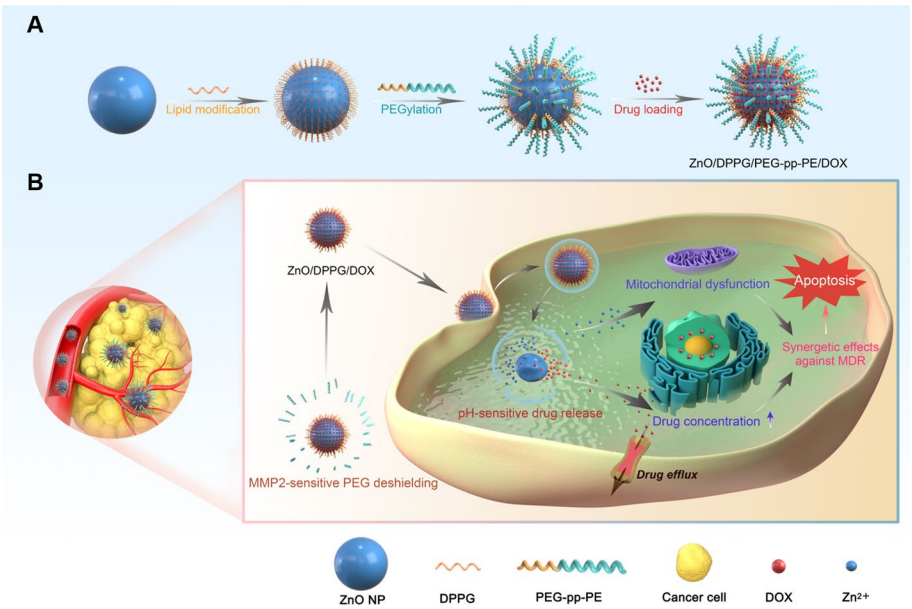

Scheme 1 **A** Preparation of the ZnO/DPPG/PEG-pp-PE/DOX NPs. **B** Schematic illustration of the MMP2 and pH dual-responsive ZnO-based polymer-lipid hybrid nanoparticles for tumor-targeted drug delivery and MDR cancer treatment

Bcl-2 (Vimala et al. 2014). Therefore, ZnO NPs may overcome the MDR of anticancer drugs.

However, the plain ZnO NPs interact with a variety of serum components and cell membrane, resulting in the rapid systemic clearance and nonspecific distribution, which limits ZnO NPs' in vivo applications. In response to these challenges, the stimuli-responsive NDDS, such as the pH, enzyme, redox potential, or external stimuli responsive systems, have emerged as a smart tumor-targeted drug delivery system (Zhou et al. 2018; Zhu and Torchilin 2013; El-Sawy et al. 2018). Among these stimuli, the overexpression of matrix metalloproteinase 2 (MMP2), which is highly associated with the tumor growth, invasion, and metastasis (Overall and López-Otín 2002), has been investigated as a robust tumor microenvironmental stimulus for the MMP2-responsive drug delivery and tumor targeting (Yao et al. 2018).

Herein, we developed a novel MMP2 and pH dual-responsive ZnO-based nanomedicine for tumor targeted drug delivery and synergistic therapy against the MDR cancer (Scheme 1). Using DOX as a model drug, the drug loading and release, physicochemical properties, stability, and sensitivity were studied. The ZnO nanomedicine's cellular uptake, spheroid penetration, and anticancer activity were evaluated in the MDR cell monolayers and three-dimensional (3D) spheroids. Finally, the DOX-loaded nanoparticles were evaluated in the MDR tumor-bearing mice in terms of their in vivo biodistribution, tumor targeting, anticancer activity, and adverse effects.

Results and discussion

ZnO NP-mediated uptake enhancement and efflux attenuation

In our previous study, we successfully loaded DOX onto the ZnO NPs and studied the influence of the ZnO NPs on DOX's anticancer activity (Wang et al. 2017).

Table 1 Particle size, zeta potential, polydispersity index (PDI), and drug (DOX) loading of the nanoparticles

Name	Particle size (nm)	PDI	Zeta potential (mV)	Drug loading (%)
ZnO	56.43 ± 12.05	0.17 ± 0.06	24.22 ± 1.32	–
ZnO/DOX	57.30 ± 9.23	0.16 ± 0.02	21.40 ± 1.89	16.28
DPPG	343.77 ± 8.04	0.27 ± 0.01	− 59.94 ± 3.20	–
ZnO/DPPG	47.05 ± 3.29	0.22 ± 0.01	− 45.30 ± 1.90	–
ZnO/DPPG/PEG-PE	60.46 ± 6.12	0.13 ± 0.02	− 16.98 ± 1.51	–
ZnO/DPPG/PEG-pp-PE	73.11 ± 10.76	0.20 ± 0.01	− 19.16 ± 3.03	–
ZnO/DPPG/PEG-PE/DOX	60.11 ± 4.43	0.19 ± 0.03	− 25.33 ± 0.54	10.33
ZnO/DPPG/PEG-pp-PE/DOX	83.25 ± 20.87	0.20 ± 0.02	− 20.43 ± 1.06	11.49

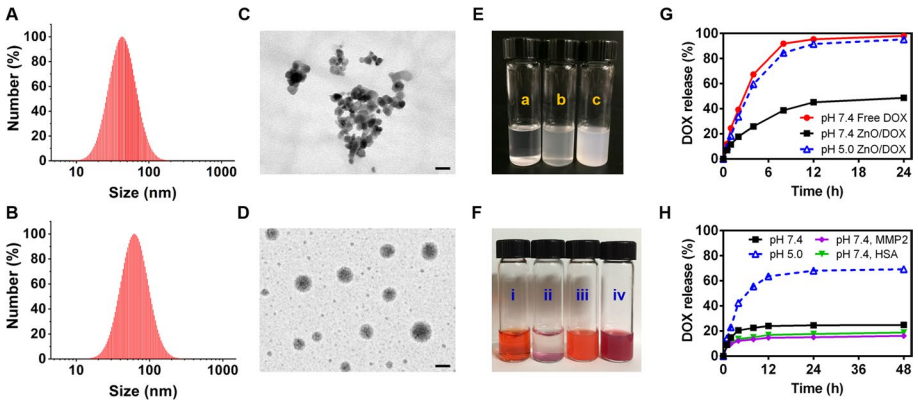

Fig. 1 Particle sizes of (**A**) ZnO/DOX and (**B**) ZnO/DPPG/PEG-pp-PE/DOX determined by the DLS. TEM images of (**C**) ZnO/DOX and (**D**) ZnO/DPPG/PEG-pp-PE/DOX, the scale bar is 100 nm. **E** Digital photographs of ZnO (a), DPPG (b), and ZnO/DPPG (c), dispersed in chloroform. (F) Digital photographs of DOX (i), ZnO/DOX (ii), ZnO/DPPG/DOX@PEG-PE (iii), and ZnO/DPPG/PEG-pp-PE/DOX (iv), dispersed in HBSS. **G** DOX release from ZnO/DOX at pH 7.4 or 5.0. **H** DOX release from ZnO/DPPG/PEG-pp-PE/DOX at pH 7.4 or 5.0, or in the presence of MMP2 or HSA

In this study, the similar method was used to load DOX onto the "plain" ZnO NPs. Therapeutic agents could be loaded onto the ZnO NPs in different ways, including the electrostatic adsorption, hydrogen bonding, and zinc-mediated chelation (Deng and Zhang 2013). Though the procedure of the DOX loading onto the ZnO NPs was simple and efficient, the exact mechanisms behind are not very clear, which may be involved in one or more aforementioned mechanisms. The dynamic light scattering (DLS) measurements showed that the average particle size of the plain ZnO NPs was 56.43 ± 12.05 nm and their zeta potential was + 24.22 ± 1.32 mV (Table 1). The loading of DOX onto the ZnO NPs didn't significantly change the NPs' particle size and zeta potential. Though the DOX-loaded ZnO NPs (ZnO/DOX) had a small particle size after the sonication or vortex (Fig. 1A), they tended to aggregate, as evidenced by the TEM images (Fig. 1C), which is unfavorable to drug delivery. Due to the strong UV interference between the zinc ions and DOX, the LC–MS/MS was used to determine the DOX content in ZnO/DOX. The drug loading efficiency of ZnO/DOX was around 16%, in consistent with the previous report (Wang et al. 2017).

The cellular uptake of ZnO/DOX was determined in the DOX-sensitive cells (MDA-MB-231 and HeLa) and MDR (DOX-resistant) cells (NCI/ADR-RES and MES-SA/Dx5). In the DOX-sensitive cells, the free DOX showed a cellular uptake 2–3 times higher than that of the ZnO/DOX (Additional file 1: Fig. S1), while in the MDR cells, the ZnO/DOX showed the enhanced cellular uptake (> 2-folds than that of the free DOX). The confocal microscopy analysis also indicated that the free DOX had higher intracellular accumulation than that of the ZnO/DOX in the MDA-MB-231 cells, while the ZnO/DOX showed much stronger intracellular fluorescence than that of the free DOX in the NCI/ADR-RES cells (Additional file 1: Fig. S2). To clarify the role of the ZnO NPs in the DOX uptake, the NCI/ADR-RES cells were pre-incubated with the ZnO NPs, followed by the DOX incubation. As shown in Additional file 1: Fig. S3, the ZnO pre-incubation could not alter the cell internalization of the DOX, suggesting that the enhanced DOX uptake of ZnO/DOX was attributed to the DOX loading onto the ZnO NPs. It is well known that the MDR cells used in the study overexpress the drug efflux pump, such as P-glycoprotein (Yao et al. 2019), lowering the intracellular concentration of various anticancer drugs, including DOX (Wang et al. 2017). The data suggested that the ZnO NPs as a nanocarrier could not only enhance the cellular uptake but also attenuate the efflux of the loaded drug (DOX) in the MDR cancer cells.

The in vitro anticancer activities of the free DOX, ZnO NPs, and ZnO/DOX were evaluated by the MTT assay. The free DOX showed the highest cytotoxicity, while the ZnO NPs showed the lowest cytotoxicity in the DOX-sensitive tumor cells (Additional file 1: Fig. S4). Here, the ZnO/DOX showed lower cytotoxicity than the free DOX, probably due to the insufficient cellular uptake (Additional file 1: Fig. S1), low intracellular drug accumulation (Additional file 1: Fig. S2), and sustained (slow) DOX release (from ZnO/DOX) (Fig. 1G). Due to the MDR, the cytotoxicity of the free DOX was remarkably decreased in the NCI/ADR-RES and MES-SA/Dx5 cells. The ZnO NPs showed cytotoxicity in both the sensitive and MDR cells, in consistent with our previous report (Wang et al. 2017). The data indicated that the efflux pump might not be unable to pump the ZnO NPs out of the cells. Unsurprisingly, the ZnO/DOX showed the highest cytotoxicity against the MDR cells, suggesting that loading of DOX onto the ZnO NPs could effectively overcome the cancer cells' MDR.

The drug penetration through the "3D" cancer cell spheroids was evaluated (Additional file 1: Fig. S7). In the MDA-MB-231 spheroids, the free DOX showed good penetration (red fluorescence) and the ZnO/DOX just slightly increased the DOX penetration compared to the free DOX, as evidenced by the overall DOX uptake (area under curve) and penetration depth (the height of peak and the distance from the bottom to the top). However, in the NCI/ADR-RES spheroids, the penetration of the free DOX was significantly decreased due to the MDR. In contrast, the ZnO/DOX showed strong fluorescence even in the "core" of the spheroids, indicating that the ZnO NPs could overcome the drug resistance (efflux) in both the monolayer cells and their 3D spheroids.

These results suggested that the ZnO NPs could be an effective drug nanocarrier against the MDR cancer cells. However, the results also suggested that the ZnO NPs possessed some "unfavorable" properties, such as the low stability, biocompatibility,

and specificity, usually resulting in the rapid systemic clearance and nonspecific biodistribution. For the successful in vivo drug delivery, the ZnO NPs need to be engineered to improve their biocompatibility, blood circulation time, and delivery specificity.

Synergistic anticancer effects of the ZnO/DOX NPs

Our previous study suggested that the ZnO NPs could induce the ROS production, leading to the death of cancer cells (Wang et al. 2017). In this study, to further evaluate the ZnO-mediated cytotoxicity, the mitochondrial membrane potential was analyzed by the membrane-permeant cationic, fluorescent carbocyanine dye (JC-1) (Liu et al. 2022). In the untreated cells with high mitochondrial transmembrane potential, JC-1 forms the J-aggregate complexes in the mitochondria and gives red fluorescence. In the treated/damaged cells, JC-1 remains in the monomeric forms in the cytosol as low mitochondrial transmembrane potential prevents its accumulation in the mitochondria and gives green fluorescence. We found that both the ZnO NPs and ZnO/DOX significantly decreased the mitochondrial membrane potential, as evidenced by the lowered Red/Green ratios (Additional file 1: Fig. S5A) and decreased red fluorescence (and the increased green fluorescence) (Additional file 1: Fig. S5B). Though DOX was reported to show mitochondrial toxicity, including the decreased membrane potential (Kuznetsov et al. 2011), the free DOX could not significantly alter the mitochondrial potential at the tested dose in the NCI/ADR-RES cells due to the MDR-induced low intracellular drug concentration (Additional file 1: Figs. S2, S3). Our data indicated that the ZnO NPs could exert cytotoxicity in cancer cells via the mitochondrial depolarization and ROS production. Interestingly, the NCI/ADR-RES cells seemed to be "tough" even after a short-time incubation with CCCP (Additional file 1: Fig. S5A). But the mechanism needs to be identified.

C/EBP homologous protein (CHOP), a pro-apoptotic transcription factor encoded by the *DDIT3* gene, plays an important role in endoplasmic reticulum (ER) stress-induced apoptosis (Oyadomari and Mori 2004). Under normal physiological conditions, CHOP is ubiquitously present at a very low level. However, under overwhelming ER stress conditions, the CHOP expression rises sharply along with the activation of apoptotic pathways in a wide variety of cells. The increase in the CHOP level is an indicator of the ER stress. Therefore, the ER stress was examined by the determination of the CHOP level in the treated NCI/ADR-RES cells. As shown in Additional file 1: Fig. S6, compared to the untreated group, no significant changes were observed in the levels of CHOP among the treatments, indicating that the ZnO NPs and DOX had the negligible effect on the ER stress in the MDR cells.

The results suggested that the ZnO NPs might enhance the DOX's cytotoxicity in the MDR cells via the increased cellular uptake, intracellular accumulation, and zinc ion-induced mitochondrial dysfunction.

Preparation and characterization of the dual-responsive ZnO/DPPG/PEG-pp-PE/DOX NPs

PEGylation has been widely used to increase the NPs' blood circulation and decrease their nonspecific interaction with the plasma proteins and mononuclear phagocyte system (MPS). By PEGylation, the NPs' tumor targetability can be improved via the tumor's

EPR effect. On the other hand, however, PEGylation may impede the cell internalization of NPs, which may not be beneficial for intracellular drug delivery. Recently, in response to this dilemma, the stimuli-responsive NDDS has emerged as a smart tumor-targeted drug delivery system. In the tumor microenvironment, certain types of MMPs are upregulated and play important roles in cancer initiation, growth, and metastasis. They have been used as the robust tumor environmental stimuli for the stimuli-responsive NDDS (Yao et al. 2018). In this study, we used the MMP2-sensitive polymer (PEG-pp-PE) to prevent the ZnO NPs from rapid systemic clearance and nonspecific distribution. In the tumor microenvironment, the peptide linker (pp) undergoes the MMP2-sensitive cleavage, resulting in the PEG deshielding and cellular uptake of the drug-loaded ZnO NPs (Scheme 1).

The synthesis of the MMP2-sensitive PEG-pp-PE was illustrated in Additional file 1: Fig. S8A. The product was characterized by the TLC and ^{1}H NMR (Fig. S8B-C), in consistent with our previous reports (Yao et al. 2017a; Liu et al. 2020). To increase the surface lipophilicity of the ZnO NPs, the anionic lipid (DPPG) was first attached on the surface of the ZnO NPs via the electrostatic adsorption (referred to ZnO/DPPG), as evidenced by the change in the zeta potential from + 24.22 (ZnO) to − 45.30 mV (ZnO/DPPG) (Table 1). We also found that the ZnO NPs failed to form a stable suspension in the chloroform and quickly settled to the bottom of the bottle, while after the DPPG modification, the ZnO/DPPG were evenly dispersed in chloroform, probably due to the increased stability (Fig. 1E).

Then, the ZnO/DPPG were PEGylated by the MMP2-sensitive PEG-pp-PE or non-sensitive PEG-PE through the emulsification and solvent evaporation method to obtain the ZnO/DPPG/PEG-pp-PE and ZnO/DPPG/PEG-PE. The DOX was readily loaded to the ZnO based NPs via the simple incubation with the doxorubicin hydrochloride solution (Wang et al. 2017) to form the ZnO/DPPG/PEG-pp-PE/DOX and ZnO/DPPG/PEG-PE/DOX, respectively. The hydrodynamic particle size and zeta potential of the ZnO NPs and their formulations were measured by the DLS in Hank's balanced salt solution (HBSS) (Table 1). The DPPG dispersion exhibited a large particle size probably due to the formation of the large liposome-like structure in water, while the ZnO NPs and their formulations had the particle sizes in the range of ~ 50–100 nm. Without the surface modification, the ZnO NPs were positively charged, and the DOX loading didn't significantly influence the NPs' zeta potential and particle sizes. In contrast, the ZnO/DPPG based NPs were negatively charged due to the anionic lipid, DPPG. The PEGylation slightly increased the ZnO/DPPG NPs' particle sizes (Fig. 1B) but lowered their negative charge from ~ − 45 mV to ~ − 20 mV, due to the PEG's steric hindrance (Table 1). The drug loading efficiency in the ZnO/DPPG/PEG-pp-PE/DOX and ZnO/DPPG/PEG-PE/DOX were 11.49% and 10.33% respectively, which was determined by the LC–MS/MS.

Stability, sensitivity and drug release of the ZnO/DPPG/PEG-pp-PE/DOX NPs

The TEM images indicated that the ZnO/DPPG/PEG-pp-PE/DOX were well dispersed in HBSS with a spherical morphology (Fig. 1D), while the ZnO/DOX showed an aggregation propensity (Fig. 1C). The ZnO/DPPG/PEG-pp-PE/DOX exhibited excellent NP stability in both the HBSS (pH 7.4) and HBSS containing 10% FBS for 72 h (Fig. 1F;

Additional file 1: Fig. S9). In our previous study, we demonstrated that the PEG-pp-PE was MMP2-sensitive and could be cleaved by MMP2 within 4 h (Liu et al. 2020). Here, to better understand the influence of the MMP2 sensitivity on the NP stability, we prolonged the MMP2 incubation time to 12 h to ensure the complete cleavage although the 1 h MMP2 incubation was sufficient to trigger the efficient cellular uptake (see Fig. 2). After the 12 h MMP2 incubation, the lose aggregates were observed in the ZnO/DPPG/PEG-pp-PE/DOX group, while the ZnO/DPPG/PEG-PE/DOX remained no change (Additional file 1: Fig. S10A). The data suggested that MMP2 could cleave PEG-pp-PE and remove the PEG shell from the NPs, resulting in the decreased NP stability in the aqueous environment. However, the MMP2-treated NPs were still in the nanometer range (< 200 nm) upon mild agitation (Additional file 1: Fig. S10B).

The drug release patterns of the ZnO/DOX and ZnO/DPPG/PEG-pp-PE/DOX were studied by the dialysis method (Wang et al. 2017). As shown in Fig. 1G, the ZnO/DOX exhibited a slow drug release rate at pH 7.4 with a < 50% DOX release at 24 h, while its drug release rate was dramatically increased at pH 5.0 with a > 90% DOX release at 10 h, which was similar to the release pattern of the free DOX. The data indicated that the DOX release from the ZnO NPs was pH-dependent due to the acidic pH-induced dissociation/dissolution of the ZnO NPs. The DPPG modification and PEGylation further slowed down the DOX release (from ZnO/DPPG/PEG-pp-PE/DOX) compared to the ZnO/DOX (Fig. 1H vs. G). However, the ZnO/DPPG/PEG-pp-PE/DOX showed a < 25% DOX release at pH 7.4 and an around 70% drug release at pH 5.0 after 48 h dialysis (Fig. 1H), indicating that these surface modifications didn't significantly influence the ZnO NPs' pH sensitivity. We also found that both the MMP2 and human serum albumin (HSA) incubation didn't significantly increase the DOX release from ZnO/DPPG/PEG-pp-PE/DOX (with a less than 20% DOX release after 48 h incubation). Although the MMP2-mediated PEG-pp-PE cleavage "released" the ZnO/DPPG/DOX resulting

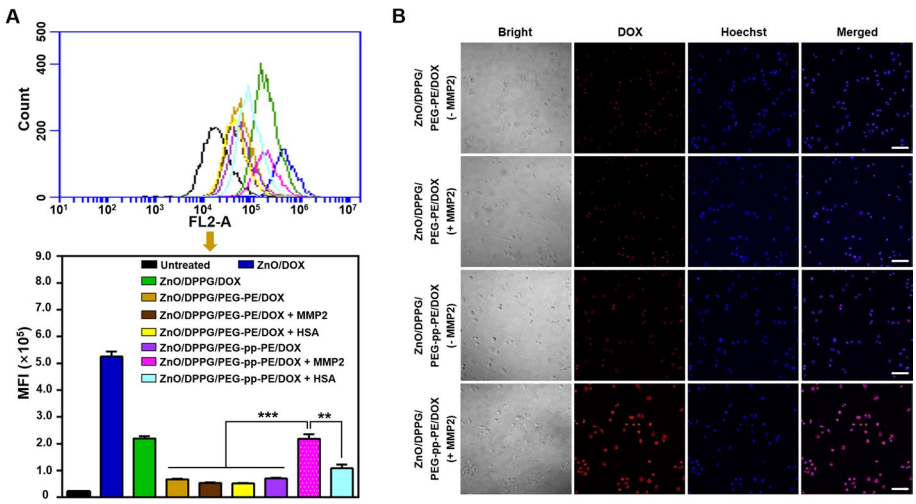

Fig. 2 **A** Cellular uptake of the DOX-loaded ZnO-based NPs after 1 h incubation with the MDR cancer cells (NCI/ADR-RES), determined by flow cytometry. MFI, mean fluorescence intensity. **B** Confocal microscopic images of cellular internalization of the ZnO/DPPG/PEG-PE/DOX and ZnO/DPPG/PEG-pp-PE/DOX with or without the MMP2 pretreatment after 1 h incubation with the NCI/ADR-RES cells. Cell nuclei were stained by Hoechst (blue). The scale bar is 100 μm. Data were expressed as the mean ± SD, $^{**}p < 0.01$; $^{***}p < 0.001$

in the slight aggregation (Additional file 1: Fig. S10A), the DOX remained "loaded" on the surface of the ZnO NPs without drug release/leakage. The high drug retention in the ZnO NPs even after the MMP2-mediated cleavage would ensure the drug's cellular uptake in the tumor microenvironment. Here, we chose the water-soluble doxorubicin hydrochloride salt instead of the insoluble DOX base to facilitate the DOX loading onto the surface of the ZnO NPs rather than the drug entrapment in the lipid (DPPG and PE) layer of the NPs, by which the DOX's pH-dependent release was secured.

Cellular uptake and penetration of the ZnO/DPPG/PEG-pp-PE/DOX NPs

The cellular uptake and penetration of the ZnO/DPPG/PEG-pp-PE/DOX were evaluated on the MDR cancer cells (NCI/ADR-RES and MES-SA/Dx5) and their 3D spheroids. After 1 h cell incubation, the ZnO/DOX exhibited the highest cellular uptake in all cancer cells due to their positive charge-triggered uptake and NP-mediated efflux inhibition (Fig. 2). The ZnO/DPPG/DOX decreased DOX's cellular uptake compared to the ZnO/DOX, probably due to the charge neutralization by DPPG. The ZnO/DPPG/PEG-PE/DOX and ZnO/DPPG/PEG-pp-PE/DOX exhibited lower cellular uptake, which might be caused by the PEG's steric hindrance. To study the impact of the MMP2-mediated cleavage on the cellular uptake, the ZnO/DPPG/PEG-PE/DOX and ZnO/DPPG/PEG-pp-PE/DOX were preincubated with MMP2 or HSA for 1 h before incubating with the cells. No significant increase in the cellular uptake was observed in the ZnO/DPPG/PEG-PE/DOX + MMP2 treated cells, while the ZnO/DPPG/PEG-pp-PE/DOX + MMP2 showed higher cellular uptake, indicating that the MMP2-mediated PEG-deshielding could enhance NPs' cellular uptake. It was worth noting that, compared with the ZnO/DPPG/PEG-PE/DOX and ZnO/DPPG/PEG-pp-PE/DOX, there was just a slight change in the cellular uptake of the ZnO/DPPG/PEG-PE/DOX + HSA and ZnO/DPPG/PEG-pp-PE/DOX + HSA, probably due to the HSA-mediated cell internalization (Hoogenboezem and Duvall 2018). In the MES-SA/Dx5 cells, the similar result that the MMP2 pre-incubation enhanced cellular uptake was observed (Additional file 1: Fig. S11A). We also noticed that the cellular uptake of the ZnO/DPPG/PEG-pp-PE/DOX + MMP2 was even higher than that of the ZnO/DPPG/DOX, probably because of the MES-SA/Dx5 cells' different response to the negatively charged ZnO/DPPG/DOX. The confocal microscopy results (Fig. 2B; Additional file 1: S11B) confirmed the flow cytometry data that the cellular uptake of the ZnO/DPPG/PEG-pp-PE/DOX was significantly enhanced after the MMP2 pre-incubation. After cell internalization, the DOX (red) was co-localized with the Hoechst (blue), which showed pink, indicating the drug accumulation in the cell nuclei.

Cancer cells cultured as the 3D cell spheroids present the similar characteristics to those of the in vivo tumor, including the morphology, growth kinetics, gene expression, drug response, etc. (Antoni et al. 2015). The cell spheroids have been also found to exhibit the drug resistance that is more relevant to the in vivo tumor as compared to the cells grown in the monolayer (Hamilton and Rath 2019). Thus, the MDR (NCI/ADR-RES) cell spheroids were established to evaluate the anti-MDR effects of the DOX-loaded NPs. The penetration of the DOX-loaded NPs through the cell spheroids was evaluated by confocal microscopy (Fig. 3). After 4 h incubation, both the ZnO/DPPG/PEG-PE/DOX and ZnO/DPPG/PEG-pp-PE/DOX showed the limited penetration in the

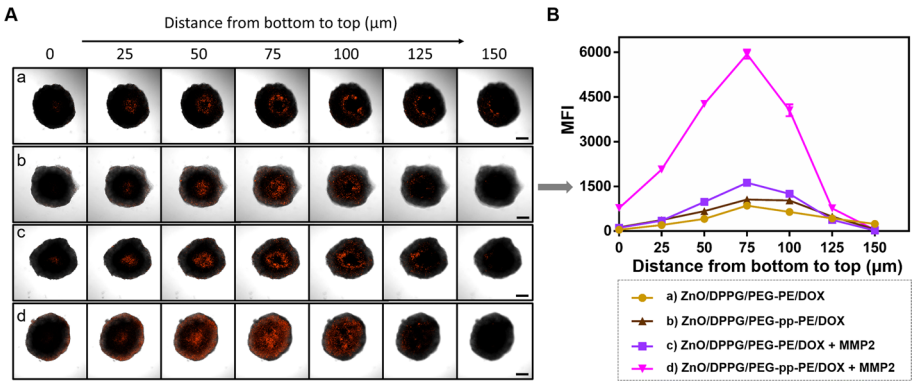

Fig. 3 **A** Drug penetration of the ZnO/DPPG/PEG-PE/DOX and ZnO/DPPG/PEG-pp-PE/DOX with/without the MMP2 pretreatment after 4 h incubation with the NCI/ADR-RES spheroids. The scale bar is 200 μm. **B** The curves of the normalized mean fluorescence intensity *vs* the distance from the spheroid bottom to the top

cell spheroids, due to the spheroid's 3D architecture, cells' drug efflux/resistance, and NPs' PEGylation (uptake inhibition) (Wang et al. 2017; Yao et al. 2019). After the MMP2 pre-incubation, the penetration ability of the ZnO/DPPG/PEG-PE/DOX + MMP2 did not significantly increase, while the ZnO/DPPG/PEG-pp-PE/DOX + MMP2 showed the enhanced spheroid penetration, as evidenced by the strong red fluorescence in the core of the spheroids.

These results suggested that, in response to the MMP2, the dual-responsive ZnO/DPPG/PEG-pp-PE/DOX could deshield the PEG shell and the exposed ZnO/DPPG/DOX NPs could enhance the tissue (spheroid) penetration and cellular uptake. Inside the cells, the ZnO was dissociated/dissolved at endosomal acidic pH, resulting in the DOX release. By this design, the efflux-mediated DOX resistance would be overcome.

In vitro cytotoxicity of the ZnO/DPPG/PEG-pp-PE/DOX NPs

In order to verify whether the enhanced cellular uptake and penetration of the ZnO/DPPG/PEG-pp-PE/DOX could lead to the increased anticancer activity, the in vitro cytotoxicity of the ZnO-based NPs on the MDR cancer cell monolayers and spheroids was evaluated by the MTT assay and CellTiter-Blue® cell viability assay. In the cell monolayers, the ZnO/DOX and ZnO/DPPG/DOX showed the highest cytotoxicity against both MDR cancer cells (NCI/ADR-RES and MES-SA/Dx5) (Fig. 4A; Additional file 1: Fig. S13, Table S1). The cytotoxicity of the ZnO/DPPG/PEG-PE/DOX didn't show the noticeable change after the MMP2 pre-incubation, while the cytotoxicity of the ZnO/DPPG/PEG-pp-PE/DOX was significantly increased. Here, the ZnO/DPPG/DOX and ZnO/DOX showed the similar cytotoxicity although the ZnO/DOX had higher cellular uptake than ZnO/DPPG/DOX, which may be attributed to the prolonged cell incubation time. Besides, we found that without the MMP2 pre-incubation, the ZnO/DPPG/PEG-pp-PE/DOX also exhibited higher cytotoxicity than the ZnO/DPPG/PEG-PE/DOX, probably because the endogenous MMP2 secreted by the cancer cells cleaved the PEG-pp-PE, leading to the increased cellular uptake (Yao et al. 2017b).

To further investigate the anticancer activity of the DOX-loaded NPs, the morphology and cell viability of the NCI/ADR-RES spheroids were determined (Additional file 1: Fig. S12; Fig. S4B). The free DOX and ZnO NPs showed mild toxicity individually while

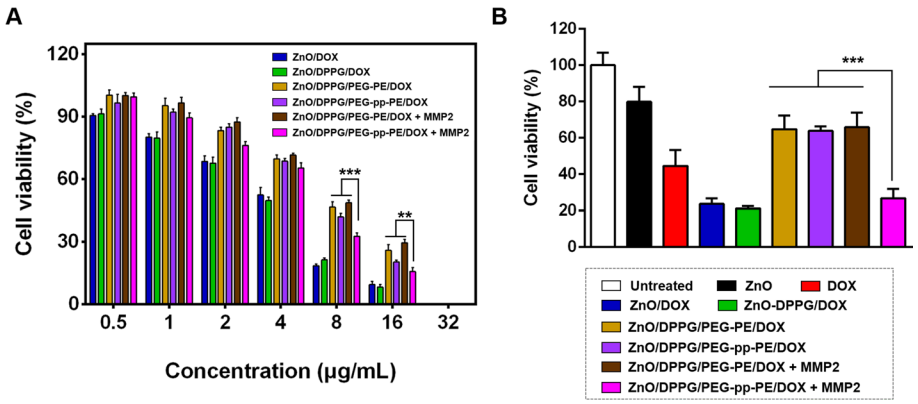

Fig. 4 **A** Cytotoxicity of the DOX-loaded ZnO-based NPs with/without the MMP2 pretreatment after 24 h incubation with the MDR cancer cells (NCI/ADR-RES). **B** Cell viability of the NCI/ADR-RES spheroids after 72 h treatments, measured by the CellTiter-Blue® Cell Viability Assay. Data were expressed as the mean ± SD, $^{**}p < 0.01$; $^{***}p < 0.001$

the DOX-loaded ZnO NPs, including the ZnO/DOX and ZnO/DPPG/DOX, exhibited the most significant toxic effects (the highest cytotoxicity and the damaged spheroid architecture) in the cancer cells, probably due to the synergistic effects of the DOX and ZnO (Additional file 1: Fig. S4; Wang et al. 2017). After the ZnO/DOX or ZnO/DPPG/DOX treatment, a blurry edge was clearly shown, which was due to the significant shedding of cells or cell debris from the spheroids (Additional file 1: Fig. S12). This was probably because of the rapid uptake (Fig. 2) and strong toxic effects (Fig. 4) of the ZnO/DOX or ZnO/DPPG/DOX on the outer layers of the cell spheroids. Without the MMP2 pre-treatment, all PEGylated NPs showed low cytotoxicity (Fig. 4) and negligible influence on the spheroid morphology (Additional file 1: Fig. S12). The MMP2 pre-treatment significantly increased the cytotoxicity of the PEG-pp-PE modified NPs (ZnO/DPPG/PEG-pp-PE/DOX + MMP2) rather than the PEG-PE modified NPs (ZnO/DPPG/PEG-PE/DOX + MMP2) (Fig. 4).

These results suggested that the DOX resistance in the MDR cancer cells and their 3D spheroids could be efficiently overcome by the dual-responsive ZnO/DPPG/PEG-pp-PE NPs, resulting in the enhanced anticancer activity.

In vivo biodistribution of the ZnO/DPPG/PEG-pp-PE/DOX NPs

The in vivo biodistribution and tumor targeting of the dual-responsive NPs were evaluated in the NCI/ADR-RES xenograft mouse model, by the live animal imaging. Due to the low tissue penetration and high absorption and emission interference of the DOX fluorescence, in this study, the Cy5.5-labeled NPs were prepared for the animal imaging (Fig. 5A). Within the 24 h upon intravenous (*i.v.*) injection, the strong fluorescence was observed in the liver and kidney in the ZnO/DOX—treated mice while no fluorescence (v.s. background) was detected in the tumor site. In contrast, the fluorescence of the liver and kidney in the ZnO/DPPG/PEG-pp-PE/DOX—treated mice was relatively low, while the fluorescence signal in the tumor was detected 2 h after *i.v.* injection. At 24 h post administration, the mice were sacrificed, and the major organs and tumor were harvested for the ex vivo fluorescence measurement (Fig. 5B). In the ZnO/

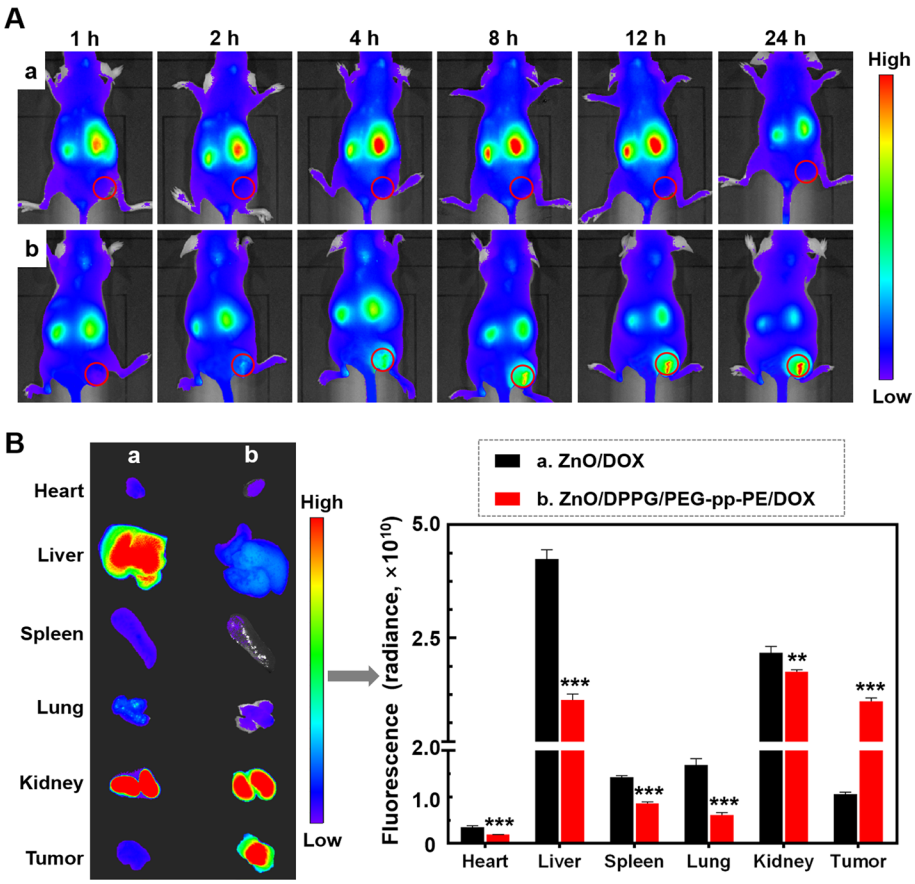

Fig. 5 **A** Biodistribution of Cy5.5-labeled ZnO/DOX (a) and ZnO/DPPG/PEG-pp-PE/DOX (b) in the NCI/ADR-RES tumor-bearing nude mice (n = 3) after intravenous injection. **B** Ex vivo fluorescent images and intensities of the excised tumors and major organs at 24 h post administration. Data were expressed as the mean ± SD, $^{**}p < 0.01$; $^{***}p < 0.001$

DOX—treated mice, the fluorescence could be observed in all major organs with the strong fluorescence in liver and kidney while the fluorescence in the tumor was negligible. In the ZnO/DPPG/PEG-pp-PE/DOX—treated mice, the fluorescence intensity was low in the excised organs except kidney, while the fluorescence in the tumor tissue was strong. These results suggested that, without PEGylation, the positively charged ZnO/DOX would be most likely opsonized and captured by the mononuclear phagocyte system (MPS), including liver and kidney, before reaching the tumor site. In contrast, the PEGylated dual-responsive ZnO/DPPG/PEG-pp-PE/DOX NPs could effectively minimize the opsonization, thus prolonging the blood circulation time and facilitating the EPR effect-mediated tumor accumulation. In addition, the MMP2-sensitive cellular uptake secured the tumor retention of the ZnO/DPPG/PEG-pp-PE/DOX.

In vivo anticancer activity of the ZnO/DPPG/PEG-pp-PE/DOX NPs

The anticancer activity of the DOX-loaded NPs was evaluated after the *i.v.* injection at 5 mg/kg DOX in the NCI/ADR-RES tumor-bearing mice. As shown in Fig. 6A, the tumor volume of the saline-treated group dramatically increased over 14 days. Compared to the saline group, the tumor growth in the free DOX or ZnO/DOX treated

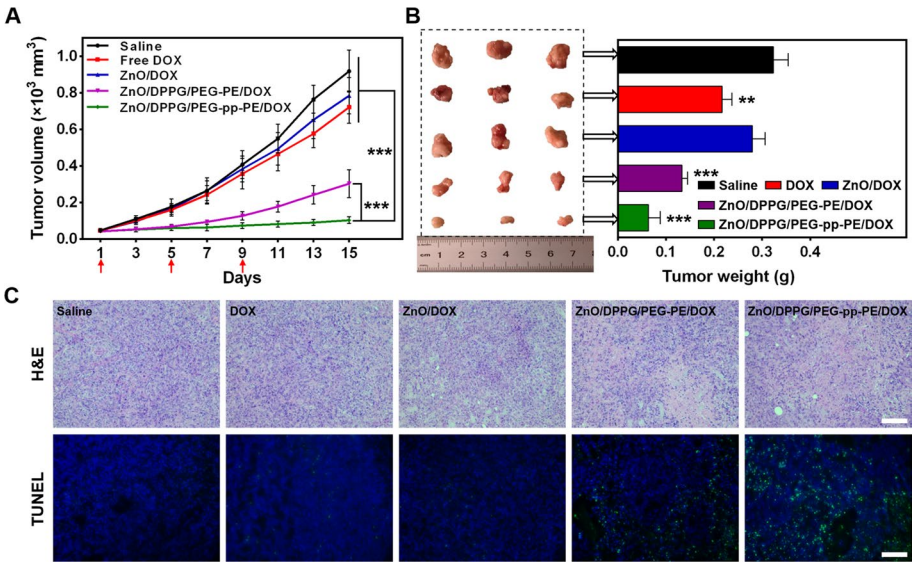

Fig. 6 **A** Tumor growth curves in the NCI/ADR-RES tumor-bearing nude mice (n = 3). **B** Images and weights of the excised tumors. **C** H&E staining and TUNEL assay of the tumor tissues. The scale bar is 100 μm. Administration: *i.v.* injection through the mouse tail vein at 5 mg·kg^{-1} DOX every 4 days for three times. Data were expressed as the mean ± SD, $^{**}p < 0.01$; $^{***}p < 0.001$

mice was just slightly inhibited, indicating their failure in the in vivo cancer treatment, although they could efficiently kill cancer cells in vitro (Fig. 4). The PEGylated NPs significantly inhibited the tumor growth, due to their long blood circulation and tumor's EPR effect. Compared to the ZnO/DPPG/PEG-PE/DOX, the dual-responsive ZnO/DPPG/PEG-pp-PE/DOX displayed higher anticancer activity. The tumor growth inhibition data were well consistent with the tumors' pictures and weights (Fig. 6B). The TUNEL assay showed that more tumor cells underwent apoptosis/necrosis in the ZnO/DPPG/PEG-pp-PE/DOX treated mice, compared to those of other treatments, which was confirmed by the H&E staining (Fig. 6C). We observed that, unlike the in vitro data, the PEGyated NPs (ZnO/DPPG/PEG-PE/DOX and ZnO/DPPG/PEG-pp-PE/DOX) exhibited a strong anticancer activity than the ZnO/DOX. The data confirmed that the ZnO/DOX was effective only in the cell cultures, whereas our dual-responsive delivery strategy could improve the in vivo biocompatibility, biodistribution, tumor targeting, and anticancer activity of the ZnO/DOX NPs.

During the study, no significant changes in the mouse body weight were observed (Fig. 7A). To study the in vivo toxicity of the treatments, the alanine aminotransferase (ALT), aspartate aminotransferase (AST), the serum creatinine (CREA), and the white blood cells (WBT) were measured (Fig. 7B). No significant changes were observed in the levels of AST and CREA among the treatments. However, compared with other treatments, the ZnO/DOX increased the ALT level and decreased the WBC. The free DOX also showed the increased toxicity though it was not statistically significant (Fig. 7B). The histological staining of the major organs including heart, liver, spleen, lung, and kidney was shown in Fig. 7C. Except for the ZnO/DOX group, other treatments didn't apparently damage the organs compared to the saline group. In the ZnO/DOX group, the inflammatory cell infiltration in the liver and the necrosis of epithelial cells in kidney

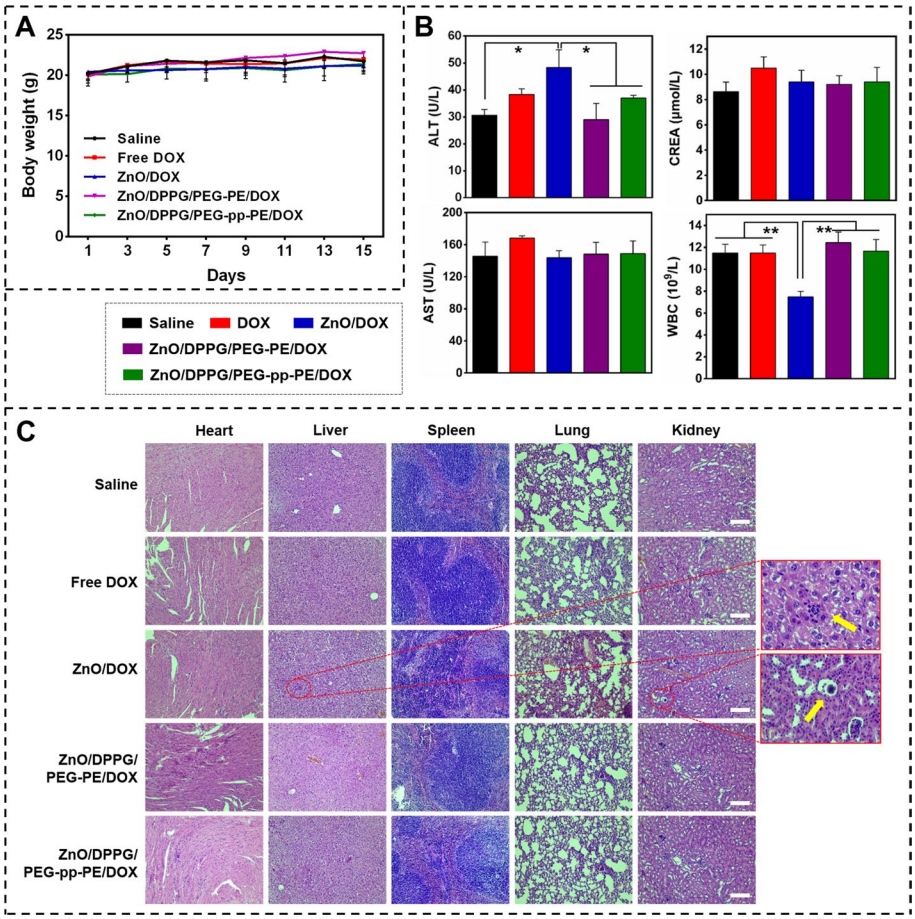

Fig. 7 **A** Mouse body weights. **B** Levels of the alanine aminotransferase (ALT), aspartate aminotransferase (AST), creatinine (CREA), and white blood cell (WBC) counts. **C** H&E staining of the vital organs after treatments. The scale bar is 100 μm. Data were expressed as the mean ± SD, $*p < 0.05$; $**p < 0.01$

tubules were found. The toxicity data indicated that the *i.v.* injection of the ZnO/DOX could result in serious hepatic and renal toxicity, and other potential side effects, which was consistent with the previous report (Esmaeillou et al. 2013). This might be caused by the ZnO/DOX's nonspecific bio-interactions and capture by the liver and kidney. In contrast, the prepared dual-responsive ZnO/DPPG/PEG-pp-PE/DOX NPs significantly improved the biocompatibility and safety of the ZnO/DOX.

Conclusion

In this study, a novel MMP2 and pH dual-responsive ZnO-based nanomedicine, ZnO/DPPG/PEG-pp-PE/DOX, was developed, which showed the excellent physicochemical properties, stability, and biocompatibility. The MMP2-sensitive tumor targeting, enhanced cellular uptake, and pH-sensitive intracellular drug release of this dual-responsive nanomedicine effectively overcame the MDR and ensured the synergistic effects of ZnO and DOX, resulting in the enhanced anticancer activity and decreased adverse effects. The developed dual-responsive ZnO-based nanomedicine held great promise for targeted drug delivery and treatment against the MDR cancer.

Methods

Preparation and characterization of the DOX-loaded ZnO NPs (ZnO/DOX)

The ZnO/DOX was prepared according to our previous study (Wang et al. 2017). Briefly, ZnO NPs (20 mg) was added into the DOX aqueous solution (5 mg/mL, 3 mL). After stirring for 24 h in the dark, the mixture was centrifuged at 12,000 rpm and washed with water for five times. The product was lyophilized by a benchtop freeze dryer (LABCONCO) to obtain ZnO/DOX. The particle size and size distribution of the ZnO/DOX were measured by the DLS on a NanoBrook 90Plus PALS Zeta Potential Analyzer (Brookhaven Instruments) at 25 °C. The NPs' zeta potential was measured by the same instrument. The morphology of the ZnO/DOX was observed via the transmission electron microscopy (TEM) (TECANI G2 Spirit BioTWIN, FEI US). The ZnO/DOX solution was pipetted on 200-mesh copper grids dropwise without staining and dried at RT before observation. Due to the UV interference of the zinc ion, a sensitive and selective LC–MS/MS method was developed to quantify DOX, which was performed on an Agilent 1260 HPLC system tandem API4000 mass system. The calibration curve for DOX was found to be linear in the concentration range of 5–5000 ng/mL, and the calibration curve regression was weighted as $1/x^2$ (x = standard concentration of DOX). The DOX concentration was calculated according to the obtained standard curve of DOX ($y = 0.227x - 0.0732$, $r = 0.9954$).

Synthesis and characterization of PEG2k-pp-PE

PEG_{2k}-pp-PE was synthesized and characterized according to our previous works (Liu et al. 2020; Yao et al. 2017b). Briefly, the PEG_{2k}-SVA was reacted with the MMP2-cleavable peptide (pp), followed by the conjugation with DOPE. The product PEG_{2k}-pp-PE was purified and obtained by the preparative TLC (chloroform/methanol, 4:1, v/v), which was then characterized by the analytical TLC and ^1H NMR spectroscopy in the deuterated chloroform.

Preparation and characterization of the dual-responsive ZnO/DPPG/PEG-pp-PE/DOX NPs

The preparation of the ZnO/DPPG/PEG-pp-PE/DOX was illustrated in Scheme 1A. First, the ZnO NPs were surface-modified by the anionic lipid DPPG (weight ratio, 1:3) by the simple incubation in chloroform overnight to form the ZnO/DPPG, followed by the addition of PEG_{2k}-PE or PEG_{2k}-pp-PE to the ZnO/DPPG chloroform mixture. Then, the organic solution was added dropwise into water, followed by a short-time sonication under the ice bath to form the emulsion. The emulsion was stirred at room temperature overnight to remove chloroform. The polymer-lipid hybrid NPs (ZnO/DPPG/PEG-PE or ZnO/DPPG/PEG-pp-PE) were formed. For drug loading, the water-soluble doxorubicin hydrochloride salt was added and incubated in dark at room temperature overnight to form the drug-loaded NPs (ZnO/DPPG/PEG-PE/DOX or ZnO/DPPG/PEG-pp-PE/DOX). The unentrapped DOX was removed by an Amicon 15 mL ultracentrifuge tube adapted with a 50 kD membrane (Merck Millipore) through centrifugation at $3000 \times g$ for 5 min. The obtained NPs were suspended in HBSS (pH 7.4) at a final concentration of 0.1 mg/mL. The particle size and size distribution of the NPs were measured by the DLS on a NanoBrook 90Plus PALS Zeta Potential Analyzer at 25 °C. The NPs' zeta potential

was measured by the same instrument. The morphology of the ZnO/DPPG/PEG-pp-PE/DOX was analyzed by the TEM. The ZnO/DPPG/PEG-pp-PE/DOX solution was pipetted on 200-mesh copper grids dropwise without staining and dried at RT before observation.

Stability and MMP2 sensitivity

To evaluate the stability, the ZnO/DPPG/PEG-pp-PE/DOX NPs were incubated in the HBSS or HBSS containing 10% FBS at 37 °C for 72 h. At the specified time intervals, the samples' particle size were measured by the DLS on a NanoBrook 90Plus PALS Zeta Potential Analyzer at 25 °C. The MMP2 sensitivity of the ZnO/DPPG/PEG-pp-PE/DOX was evaluated by the enzymatic digestion using the MMP2. Briefly, the ZnO/DPPG/PEG-pp-PE/DOX NPs were incubated with 50 μg/mL MMP2 for 12 h, and thereafter the treated samples were mildly agitated and their particle sizes were measured. In addition, the digital photographs of the ZnO/DPPG/PEG-PE/DOX and ZnO/DPPG/PEG-pp-PE/DOX were taken.

In vitro drug release

The DOX release from the ZnO/DOX and ZnO/DPPG/PEG-pp-PE/DOX was studied by the dialysis method. Briefly, 1 mL of the ZnO/DOX suspension (1 mg/mL) was dialyzed (MWCO: 3.5 kDa) against 100 mL of the HBSS (pH 7.4 or 5.0) at 37 °C. At the specified time intervals, 100 μL of the external medium was collected and replaced by the same volume of the fresh HBSS. For the ZnO/DPPG/PEG-pp-PE/DOX, 1 mL of the ZnO/DPPG/PEG-pp-PE/DOX suspension (2 mg/mL) was dialyzed (MWCO: 3.5 kDa) against 100 mL of the HBSS (pH 7.4 or 5.0, with MMP2 or HSA) at 37 °C. The DOX in the external medium was determined by the LC–MS/MS method.

Cellular uptake determined by flow cytometry

The cellular uptake of the DOX and DOX-loaded NPs was determined in the DOX-sensitive cancer cells (MDA-MB-231 and HeLa) and MDR cancer cells (NCI/ADR-RES and MES-SA/Dx5) by flow cytometry. Briefly, the cells were seeded into 6-well plates at a density of 3×10^5 cells/well and incubated overnight, followed by the incubation with the DOX or DOX-loaded NPs at 8 μg/mL DOX for 1 h. Then, the cells were harvested by trypsinization and centrifugation at 1000 rpm for 5 min, and resuspended in 500 μL of HBSS and analyzed by a BD Accuri C6 flow cytometer. The untreated cells were served as the negative control. To study the role of the ZnO NPs on the DOX uptake, the NCI/ADR-RES cells were pre-incubated with the ZnO NPs for 1 h, followed by the DOX incubation. To study the impact of the MMP2-mediated cleavage on the cellular uptake, the ZnO/DPPG/PEG-PE/DOX or ZnO/DPPG/PEG-pp-PE/DOX NPs were pre-incubated with 50 μg/mL MMP2 or HSA at 37 °C for 1 h.

Intracellular distribution determined by confocal microscopy

To observe the intracellular distribution and the fluorescence intensity of the DOX and DOX-loaded NPs, we used confocal microscopy. For this purpose, the cells were seeded into 6-well plates at a density of 3×10^5 cells/well and incubated overnight, followed by the incubation with the DOX or DOX-loaded NPs at 8 μg/mL DOX for 1 h. Then,

the cells were washed by HBSS and fixed in 4% paraformaldehyde for 10 min, followed by Hoechst 33,258 staining for 15 min. After washing with HBSS, the cells were analyzed using a Nikon eclipse 80i confocal microscope system. To study the impact of the MMP2-mediated cleavage on cellular uptake, the ZnO/DPPG/PEG-PE/DOX or ZnO/DPPG/PEG-pp-PE/DOX NPs were preincubated with 50 μg/mL MMP2 at 37 °C for 1 h.

Establishment of cancer cell spheroids

The cancer cell spheroids were established according to our previous reports (Wang et al. 2017; Yao et al. 2017a, 2017b; Liu et al. 2020). First, the 96-well plate was pre-coated with the agarose in the culture medium (1.5%, w/v), followed by gelation at the room temperature. The cells were seeded in the pre-coated plates at 8×10^3 cells/well (200 μL). The plates were then centrifuged for 15 min at 1500 rcf and incubated at 37 °C in 5% CO_2 for the formation of cell spheroids.

Drug penetration through cancer cell spheroids

The 4-day old cell spheroids with a diameter of 400–600 μm were used to study the drug penetration. The DOX or DOX-loaded NPs at 8 μg/mL DOX were incubated with the cell spheroids for 4 h. Then, the spheroids were transferred to a new well and gently washed with HBSS, followed by confocal microscopy. The Z-stack images were obtained at the fixed interval of 25 μm. The fluorescence intensity of the selected images was analyzed by the ImageJ software. The mean fluorescence intensity (MFI) was plotted against the distance. To study the impact of the MMP2 sensitivity on the drug's spheroid penetration, the ZnO/DPPG/PEG-PE/DOX or ZnO/DPPG/PEG-pp-PE/DOX NPs were preincubated with 50 μg/mL MMP2 at 37 °C for 1 h.

Cytotoxicity in cancer cell monolayers

The cytotoxicity of the NPs in the cancer cells, including MDA-MB-231, Hela, NCI/ADR-RES, and MES-SA/Dx5, were investigated by the MTT assay. In brief, the cells were seeded into 96-well plates at 5×10^3 cells/well and incubated at 37 °C overnight before the treatment. The free DOX, ZnO NPs, ZnO/DOX, or other NPs were incubated with the cells at the DOX concentrations of 0.5–50 μg/mL for 24 h. The MTT solution (5 μg/μL) was diluted by the cell medium by 10 folds and incubated with cells for 4 h. Then, the medium was removed and 150 μL DMSO was added. The absorbance was determined at 570 nm with a reference wavelength of 630 nm on a microplate reader. To study the impact of the MMP2 sensitivity on the cytotoxicity, the NPs were preincubated with 50 μg/mL MMP2 or HSA at 37 °C for 1 h.

Cytotoxicity in cancer cell spheroids

The cell spheroids were incubated with the ZnO NPs, DOX or DOX-loaded NPs in the complete growth medium for 72 h. The spheroids' morphology was recorded by a microscope at 0 h, 4 h, 8 h, 12 h, 24 h, 48 h and 72 h to estimate the spheroid growth inhibition. After 72 h treatments, the cell viability of the spheroids was determined by the CellTiter-Blue® Cell Viability Assay. Briefly, 20 μL of the reagent was diluted with 180 μL of the complete growth medium and incubated with the cell spheroids at 37 °C

for 12 h. Thereafter, the fluorescence intensity (λ_{ex} 560 nm, λ_{em} 590 nm) was measured by a microplate reader.

Determination of the mitochondrial membrane potential (JC-1 assay)

For the mitochondrial membrane potential analysis, the cells were seeded at a density of 2×10^5 cells/well in 12-well plates for 24 h. Then, the cells were incubated with the ZnO (10, 20, and 30 μg/mL), DOX (4 μg/mL), ZnO/DOX (20 μg/mL/4 μg/mL), and mitochondrial uncoupler, carbonyl cyanide 3-chlorophenylhydrazone (CCCP) (50 μM), respectively. The cells were washed by the ice-cold medium to remove the uninternalized materials and then incubated with the JC-1 dye at 37 °C for 20 min, followed by flow cytometry and confocal microscopy. The confocal microscopy analysis was carried out in the simultaneous mode for red ($\lambda_{ex} = 525$ nm) and green emission ($\lambda_{ex} = 488$ nm).

Determination of the ER stress (CHOP assay)

The cells were seeded at a density of 2×10^5 cells/well in 12-well plates for 24 h. The cells were incubated with the ZnO (10, 20, and 30 μg/mL), DOX (4 μg/mL), ZnO/DOX (20 μg/mL/4 μg/mL) for 24 h, respectively. The CHOP levels were measured using a commercially available enzyme-linked immunosorbent assay (ELISA) kit according to the manufacturer's protocol.

In vivo imaging

The in vivo biodistribution of the ZnO/DOX and ZnO/DPPG/PEG-pp-PE/DOX NPs was analyzed by the IVIS spectrum imaging system. To track the drug biodistribution, the NIR probe Cy5.5 was covalently conjugated to the DOX. Briefly, 5 mg of Cy5.5-NHS were reacted with DOX (5 mg) in 5 mL DMF (2% TEA contained). After stirring for 24 h at room temperature, the solution was dialyzed against water (MWCO: 1 kD), and then freeze-dried to obtain the dark blue powder. When the tumor was around 400 mm^3, the Cy5.5 labeled ZnO/DOX or ZnO/DPPG/PEG-pp-PE/DOX were intravenously injected in the mice via the tail vein (Cy5.5: 0.1 mg/kg). The fluorescence at 1 h, 2 h, 4 h, 8 h, 12 h, and 24 h upon injection were recorded. At 24 h post administration, the mice were sacrificed, and the major organs and tumors were excised to analyze the ex vivo fluorescence.

In vivo anticancer activity

For the tumor growth inhibition study, the NCI/ADR-RES tumor-bearing mice were randomly divided into five groups with three mice per group. When the tumor volume reached around 50 mm^3, the mice were treated by the saline, free DOX, ZnO/DOX, ZnO/DPPG/PEG-PE/DOX, or ZnO/DPPG/PEG-pp-PE/DOX via *i.v.* injection at the DOX dose of 5 mg/kg body weight every 4 days (3 injections in total). The tumor volume was measured every two days upon the treatments and calculated by the equation $V = (l \times w^2)/2$, where "l" is the tumor length and "w" is the tumor width. The mouse body weight was also measured to evaluate the systemic toxicity. On the 14th day upon the treatments, the mice were sacrificed, and the blood, major organs, and tumors were collected. The excised tumors were weighed. The alanine aminotransferase (ALT), aspartate aminotransferase (AST), and the serum creatinine (CREA) were measured by the assay

kits (Teco Diagnostics, Anaheim, CA, USA). The white blood cells (WBC) were counted by a hemocytometer.

Histological analysis

Histological staining was carried out on the 14th day of the treatments. The major organs, including heart, liver, spleen, lung, and kidney, and tumors of the mice were harvested. The tissues were dehydrated using the buffered formalin, ethanol, and xylene. Then, the samples were embedded in the liquid paraffin. The sliced samples (3–5 μm) were stained with hematoxylin and eosin (H&E) and examined by microscopy. In addition, the paraffin-embedded tumor sections were analyzed by the terminal transferase dUTP nick-end labeling (TUNEL) assay.

Statistical analysis

The data were presented as mean ± SD and performed by a one-way ANOVA analysis, using the GraphPad Prism v6.00. P values < 0.05 were considered statistically significant. $^{*}p < 0.05$, $^{**}p < 0.01$, $^{***}p < 0.001$.

Supplementary Information

The online version contains supplementary material available at https://doi.org/10.1186/s12645-023-00205-7.

Additional file 1. Fig. S1. Cellular uptake of the DOX or ZnO/DOX in the DOX-sensitive cancer cells and DOX-resistant MDR cancer cells after 1 h incubation, determined by flow cytometry. Mean fluorescence intensity of the flow cytometry data. **Fig. S2.** Confocal microscopic images of cellular internalization of the DOX or ZnO/DOX in the MDA-MB-231 and NCI/ADR-RES cells after 1 h incubation. Cell nuclei were stained by Hoechst. The scale bar is 100 μm. **Fig. S3.** Uptake of the DOX, ZnO/DOX, or ZnO + DOX mixture after 1 h incubation with the MDR cancer cells, determined by flow cytometry. MFI, mean fluorescence intensity. **Fig. S4.** Cytotoxicity of the DOX, ZnO NPs, and ZnO/DOX in DOX-sensitive cancer cells and DOX-resistant MDR cancer cells. Cell incubation time: 24 h. **Fig. S5.** Mitochondrial membrane potential after 1 h or 24 h treatments, determined by the JC-1 assay. The decrease in the JC-1 aggregate/monomer ratio indicates the mitochondrial depolarization. Confocal microscopic images of the JC-1 staining after 4 h treatments. The scale bar is 50 μm. **Fig. S6.** The C/EBP Homologous Protein levels after 24 h treatments, determined by a CHOP ELISA kit. Cell line: NCI/ADR-RES cells. **Fig. S7.** Drug penetration through the MDA-MB-231 and NCI/ADR-RES cell spheroids after 4 h incubation, determined by confocal microscopy. The scale bar is 200 μm. The right panel is the curves of the normalized mean fluorescence intensity vs the distance from the spheroid bottom to the top. **Fig. S8.** Synthetic scheme of the PEG-pp-PE.TLC chromatograms of the PEG-pp and PEG-pp-PE.^{1}H NMR spectrum of the PEG-pp-PE. **Fig. S9.** Mean particle sizes of the ZnO/DPPG/PEG-pp-PE/DOX upon the incubation with HBSS or HBSS containing 10% FBS for 72 h. Particle sizes were measured by dynamic light scattering. **Fig. S10.** Digital photographs of the ZnO/DPPG/PEG-PE/DOX and ZnO/DPPG/PEG-pp-PE/DOX with the MMP2 incubation for 12 h. Particle sizes of the ZnO/DPPG/PEG-pp-PE/DOX with/without the MMP2 pretreatment, determined by dynamic light scattering. **Fig. S11.** Cellular uptake of the DOX-loaded ZnO-based NPs in the MDR cancer cells after 1 h incubation, determined by flow cytometry. MFI, mean fluorescence intensity. Confocal microscopic images of the cellular internalization of ZnO/DPPG/PEG-PE/DOX and ZnO/DPPG/PEG-pp-PE/DOX with or without the MMP2 pretreatment after 1 h incubation with the MES-SA/Dx5 cells. Cell nuclei were stained by Hoechst. The scale bar is 100 μm. Data were expressed as the mean ± SD, $^{**}p < 0.01$; $^{***}p < 0.001$. **Fig. S12.** Morphology of the NCI/ADR-RES cell spheroids after treatments. The scale bar is 200 μm. **Fig. S13.** Cytotoxicity of the DOX-loaded ZnO-based NPs with/without the MMP2 pretreatment after 24 h incubation with the MDR cancer cells. Data were expressed as the mean ± SD, $^{**}p < 0.01$; $^{***}p < 0.001$.

Acknowledgements
Not applicable.

Author contributions
LZ, HW, and QZ designed the research; QZ, LZ, YJL and XLH performed the experiments; JW, JYZ and YBQ analyzed the data; LZ, HW, and QZ wrote the paper. All authors have reviewed the manuscript. All authors read and approved the final manuscript.

Funding
The work was supported by the National Natural Science Foundation of China (No. 81901890 to Qing Zhou and 82101063 to Li Zhang), the Natural Science Foundation of Jiangsu Province (No. BK20200147 to Li Zhang), and the Innovation Capability Support Plan of Shaanxi Province (No. 2020TD-041 to Hong Wu). Qing Zhou is also grateful to the China Scholarship Council (CSC) for the financial support (CSC number 201603170199).

Availability of data and materials
The data that support the findings of this study are available from the corresponding authors upon reasonable request.

Declarations

Ethics approval and consent to participate
All animal experiments and tests were guided and approved by the Animal Care Committee of Jinling Hospital.

Consent for publication
All authors agree to the publication of this manuscript.

Competing interests
The authors have declared that no competing interest exists.

Received: 6 March 2023 Accepted: 25 April 2023
Published online: 20 May 2023

References

Adir O, Poley M, Chen G, Froim S, Krinsky N, Shklover J, Shainsky-Roitman J, Lammers T, Schroeder A (2020) Integrating artificial intelligence and nanotechnology for precision cancer medicine. Adv Mater 32(13):1901989
An X, Sarmiento C, Tan T, Zhu H (2017) Regulation of multidrug resistance by microRNAs in anti-cancer therapy. Acta Pharm Sin b 7(1):38–51
Anjum S, Hashim M, Malik SA, Khan M, Lorenzo JM, Abbasi BH, Hano C (2021) Recent advances in zinc oxide nanoparticles (Zno nps) for cancer diagnosis, target drug delivery, and treatment. Cancers 13(18):4570
Antoni D, Burckel H, Josset E, Noel G (2015) Three-dimensional cell culture: a breakthrough in vivo. Int J Mol Sci 16(3):5517–5527
Bisht G, Rayamajhi S (2016) ZnO nanoparticles: a promising anticancer agent. Nanobiomedicine 3:3–9
Bukowski K, Kciuk M, Kontek R (2020) Mechanisms of multidrug resistance in cancer chemotherapy. Int J Mol Sci 21(9):3233
Chaturvedi VK, Singh A, Singh VK, Singh MP (2019) Cancer nanotechnology: a new revolution for cancer diagnosis and therapy. Curr Drug Metab 20(6):416–429
Chauhan PS, Bhushan B, Singh L, Mishra AK, Saluja S, Mittal V, Gupta DK, Kapur S (2012) Expression of genes related to multiple drug resistance and apoptosis in acute leukemia: response to induction chemotherapy. Exp Mol Pathol 92(1):44–49
David CA, Galceran J, Rey-Castro C et al (2012) Dissolution kinetics and solubility of ZnO nanoparticles followed by AGNES. J Phys Chem C 116(21):11758–11767
Deng Y, Zhang H (2013) The synergistic effect and mechanism of doxorubicin-ZnO nanocomplexes as a multimodal agent integrating diverse anticancer therapeutics. Int J Nanomed 8:1835
El-Sawy HS, Al-Abd AM, Ahmed TA, El-Say KM, Torchilin VP (2018) Stimuli-responsive nano-architecture drug-delivery systems to solid tumor micromilieu: past, present, and future perspectives. ACS Nano 12(11):10636–10664
Esmaeillou M, Moharamnejad M, Hsankhani R, Tehrani AA, Maadi H (2013) Toxicity of ZnO nanoparticles in healthy adult mice. Environ Toxicol Pharmacol 35(1):67–71
Guo D, Wu C, Jiang H, Li Q, Wang X, Chen B (2008) Synergistic cytotoxic effect of different sized ZnO nanoparticles and daunorubicin against leukemia cancer cells under UV irradiation. J Photochem Photobiol B, Biol 93(3):119–126
Hamilton G, Rath B (2019) Applicability of tumor spheroids for in vitro chemosensitivity assays. Expert Opin Drug Metab Toxicol 15(1):15–23
Hoogenboezem EN, Duvall CL (2018) Harnessing albumin as a carrier for cancer therapies. Adv Drug Delivery Rev 130:73–89
Iwamoto T (2013) Clinical application of drug delivery systems in cancer chemotherapy: review of the efficacy and side effects of approved drugs. Biol Pharm Bull 36(5):715–718
Kunjachan S, Rychlik B, Storm G, Kiessling F, Lammers T (2013) Multidrug resistance: physiological principles and nanomedical solutions. Adv Drug Deliv Rev 65(13–14):1852–1865
Kuznetsov AV, Margreiter R, Amberger A, Saks V, Grimm M (2011) Changes in mitochondrial redox state, membrane potential and calcium precede mitochondrial dysfunction in doxorubicin-induced cell death. Biochim Biophys Acta 1813(6):1144–1152
Liu Y, Wang J, Zhang J, Marbach S, Xu W, Zhu L (2020) Targeting tumor-associated macrophages by MMP2-sensitive apoptotic body-mimicking nanoparticles. ACS Appl Mater Interfaces 12(47):52402–52414
Liu S, Khan AR, Yang X, Dong B, Ji J, Zhai G (2021) The reversal of chemotherapy-induced multidrug resistance by nanomedicine for cancer therapy. J Control Release 335:1–20
Liu Y, Zhang J, Tu Y, Zhu L (2022) Potential-independent intracellular drug delivery and mitochondrial targeting. ACS Nano 16(1):1409–1420
Misra R, Acharya S, Sahoo SK (2010) Cancer nanotechnology: application of nanotechnology in cancer therapy. Drug Discov Today 15(19–20):842–850
Modok S, Mellor HR, Callaghan R (2006) Modulation of multidrug resistance efflux pump activity to overcome chemoresistance in cancer. Curr Opin Pharmacol 6(4):350–354
Montazami N, Aghapour M, Farajnia S, Baradaran B (2015) New insights into the mechanisms of multidrug resistance in cancers. Cell Mol Biol 61(7):70–80

Overall CM, López-Otín C (2002) Strategies for MMP inhibition in cancer: innovations for the post-trial era. Nat Rev Cancer 2(9):657–672
Oyadomari S, Mori M (2004) Roles of CHOP/GADD153 in endoplasmic reticulum stress. Cell Death Differ 11(4):381–389
Patel NR, Pattni BS, Abouzeid AH, Torchilin VP (2013) Nanopreparations to overcome multidrug resistance in cancer. Adv Drug Deliv Rev 65(13–14):1748–1762
Pluchino KM, Hall MD, Goldsborough AS, Callaghan R, Gottesman MM (2012) Collateral sensitivity as a strategy against cancer multidrug resistance. Drug Resist Updat 15(1–2):98–105
Pugazhendhi A, Edison TNJI, Velmurugan BK, Jacob JA, Karuppusamy I (2018) Toxicity of Doxorubicin (Dox) to different experimental organ systems. Life Sci 200:26–30
Robey RW, Pluchino KM, Hall MD, Fojo AT, Bates SE, Gottesman MM (2018) Revisiting the role of ABC transporters in multidrug-resistant cancer. Nat Rev Cancer 18(7):452–464
Somu P, Paul S (2019) A biomolecule-assisted one-pot synthesis of zinc oxide nanoparticles and its bioconjugate with curcumin for potential multifaceted therapeutic applications. New J Chem 43(30):11934–11948
Su Z, Dong S, Zhao S-C, Liu K, Tan Y, Jiang X, Assaraf YG, Qin B, Chen Z-S, Zou C (2021) Novel nanomedicines to overcome cancer multidrug resistance. Drug Resist Updat 58:100777
Szakács G, Paterson JK, Ludwig JA, Booth-Genthe C, Gottesman MM (2006) Targeting multidrug resistance in cancer. Nat Rev Drug Discov 5(3):219–234
van den Boogaard WM, Komninos DS, Vermeij WP (2022) Chemotherapy side-effects: not all DNA damage is equal. Cancers 14(3):627
Vimala K, Sundarraj S, Paulpandi M, Vengatesan S, Kannan S (2014) Green synthesized doxorubicin loaded zinc oxide nanoparticles regulates the Bax and Bcl-2 expression in breast and colon carcinoma. Process Biochem 49(1):160–172
Wang J, Lee JS, Kim D, Zhu L (2017) Exploration of zinc oxide nanoparticles as a multitarget and multifunctional anticancer nanomedicine. ACS Appl Mater Interfaces 9(46):39971–39984
Wiesmann N, Tremel W, Brieger J (2020) Zinc oxide nanoparticles for therapeutic purposes in cancer medicine. J Mater Chem B 8(23):4973–4989
Yao Q, Dai Z, Hoon Choi J, Kim D, Zhu L (2017a) Building stable MMP2-responsive multifunctional polymeric micelles by an all-in-one polymer-lipid conjugate for tumor-targeted intracellular drug delivery. ACS Appl Mater Interfaces 9(38):32520–32533
Yao Q, Choi JH, Dai Z, Wang J, Kim D, Tang X, Zhu L (2017b) Improving tumor specificity and anticancer activity of dasatinib by dual-targeted polymeric micelles. ACS Appl Mater Interfaces 9(42):36642–36654
Yao Q, Kou L, Tu Y, Zhu L (2018) MMP-responsive 'smart' drug delivery and tumor targeting. Trends Pharmacol Sci 39(8):766–781
Yao Q, Liu Y, Kou L, Tu Y, Tang X, Zhu L (2019) Tumor-targeted drug delivery and sensitization by MMP2-responsive polymeric micelles. Nanomedicine 19:71–80
Zhou Q, Zhang L, Yang T, Wu H (2018) Stimuli-responsive polymeric micelles for drug delivery and cancer therapy. Int J Nanomedicine 13:2921
Zhu L, Torchilin VP (2013) Stimulus-responsive nanopreparations for tumor targeting. Integr Biol 5(1):96–107

Publisher's Note